

Non-Gaussian statistics and extreme events on experimental fracture surfaces

Yuanyuan Cao¹, Stéphane Vernède^{2,3} and Laurent Ponson^{1,*}

¹ *Institut Jean Le Rond d'Alembert (UMR 7190), CNRS - UPMC Université Paris 06, 75005 Paris, France.*

² *EO Technology, Fengrun Building 606, 280 Heping North Road, 213000 Changzhou, China.*

³ *Baseline Consulting Services (Shanghai) Co., A-401, 125 Jiangsu North Road, 200042 Shanghai, China;*

* *Corresponding author : laurent.ponson@upmc.fr*

Abstract: Experimental studies show that fracture surfaces exhibit rather remarkable scaling properties characterized by universal roughness exponents, close to $\zeta = 0.4$ in brittle materials and close to $\zeta = 0.8$ in quasi-brittle and ductile materials. In this work, we go beyond the value of the roughness exponent, and focus on the distribution of height fluctuations on the fracture surface of a large range of materials, from brittle to ductile and quasi-brittle solids. At first, we show how damage accompanying crack propagation results on average into deviations to the Gaussian statistics observed on brittle fracture surfaces. Then, we identify on the fracture surface the location of the largest jumps responsible for the fat tails observed on these distributions, and show that these extreme events are actually organized in a network of clusters made of connected events. The statistical analysis of these clusters show many interesting features, including a characteristic sizes reminiscent of the typical size of the damage processes in the material studied, a power law distribution of cluster size for ductile and quasi-brittle fracture surface, while their probability distribution decay exponentially in brittle fracture surface. This new approach in the analysis of the morphology of fracture surface is a first step into a better understanding of the damage processes occurring within the process zone during crack propagation, and open promising perspectives into the description of damage mechanisms in a large range of materials by an unified theory.

Keywords: Fracture surface, roughness statistics, scaling behavior.

1 Introduction

Understanding the failure properties of a solid is a constant goal in material science. A fine description of these properties can have important applications for the design of new materials and the expertise of failures. Experimental studies show that fracture surfaces exhibit rather remarkable scaling properties characterized by universal roughness exponents, close to $\zeta = 0.4$ in brittle materials and close to $\zeta = 0.8$ in quasi-brittle and ductile materials. However, much more information about the failure process remains encoded in the fracture surface as the crack roughness reveals the interaction between the crack fronts and the material microstructure. Therefore a fine description of the statistics of fracture surface shall guide the development of more accurate models of fracture propagation and therefore allows a finer understanding of the failure process.

2 Material and methods

Aluminum alloy and mortar are chosen as the archetypes of ductile and quasi-brittle materials, respectively. The alloy specimens are aluminum 4 wt% copper with an as-casted microstructure. They are broken under uniaxial mode I tension with constant traction velocity (strain rate of approximately $1.6 \times 10^{-2} \text{s}^{-1}$) [1]. Their fracture surfaces are observed with a scanning electron microscope at two tilt angles. A high resolution elevation map is produced from the stereo pair using the cross-correlation based surface reconstruction technique. The reconstructed image of the topography represents a rectangular field of $3.7 \times 2.7 \text{ mm}$ (1250×950 pixels). The in-plane and out-of-plane resolutions are of the order of $3 \mu\text{m}$. We present results for sample broken at different temperatures, i.e. 480° for the sample #1 and 620°C for the sample #2. A part of the fracture surface of aluminum #2 ($2.7 \times 2.7 \text{ mm}$) is represented on Fig. 1(a). Mortar fracture surfaces are obtained by applying four points bending under controlled displacement conditions to a notched beam. The length of the beam is 1400 mm and its height and thickness are both equal to 140 mm. The topography of the fracture surfaces is recorded using an optical profilometer. The maps include 400 profiles of 4096 points each. We make sure that the analyzed profiles are located far enough from the initiation region, so that the roughness properties are statistically stationary. The sampling step along profiles is $20 \mu\text{m}$. Two successive profiles are separated by $50 \mu\text{m}$ along the direction of crack propagation. The lateral and vertical accuracy are of the order of $5 \mu\text{m}$ (see [2] for more experimental details). A part of the fracture surface #2 ($20 \times 20 \text{ mm}$) is represented on Fig. 1(b). In situ observations and acoustic emissions analysis show that failure occurs by multicracking processes present in an extended zone ahead of the notch. To compare our findings with a reference material that does not involve damage mechanisms, fracture surfaces of brittle ceramics made of sintered glass beads are also analyzed. For this material, the process zone was shown to be much smaller than the diameter $d \simeq 100 \mu\text{m}$ of the grains [12]. Tapered Double Cantilever Beam with width and length equal to 20 mm (perpendicular to the crack propagation) and 60 mm (parallel to it) respectively, are broken at constant opening rate. The tapered shape of these specimens allows us to obtain a stable quasi-static mode I crack growth. The roughness of the fractured specimens is measured using a mechanical stylus profilometer (TMTalysurf Intra) with a 10 nm vertical and a $2 \mu\text{m}$ lateral resolutions. The obtained fracture surface ($8 \times 8 \text{ mm}$) is shown on Fig. 1(c).

3 Non-Gaussian statistics of fracture surface roughness

We first study the distribution of height fluctuation on the fracture surfaces. For a given increment $\delta\vec{x}$ of the coordinates in the average fracture plane, we note $p(\delta h|\delta\vec{x})$ the probability distribution of an height increment $\delta h = h(\vec{x}) - h(\vec{x} + \delta\vec{x})$ where the sampling of the distribution is done on all admissible coordinates \vec{x} . We also note $p(\delta h|\delta r)$ the distribution of δh where the sampling is done on all admissible \vec{x} and $\delta\vec{x}$ such as $|\delta\vec{x}| = \delta r$. The distribution $p(\delta h|\delta r)$ at different δr is shown in a semi-logarithmic scale on Fig. 2 for (a) aluminum alloy sample #2, (b) For the aluminum and mortar samples (Fig. 2(a)(b)), the distribution of height fluctuations shows a strong non-Gaussian behavior at small scale δr with pronounced fat tail. As the scale δr is increased, the tails of the distribution become less pronounced. At a sufficiently large scale, the distribution can barely be distinguished from a Gaussian distribution, taking a parabolic shape in this semi-logarithmic representation. For

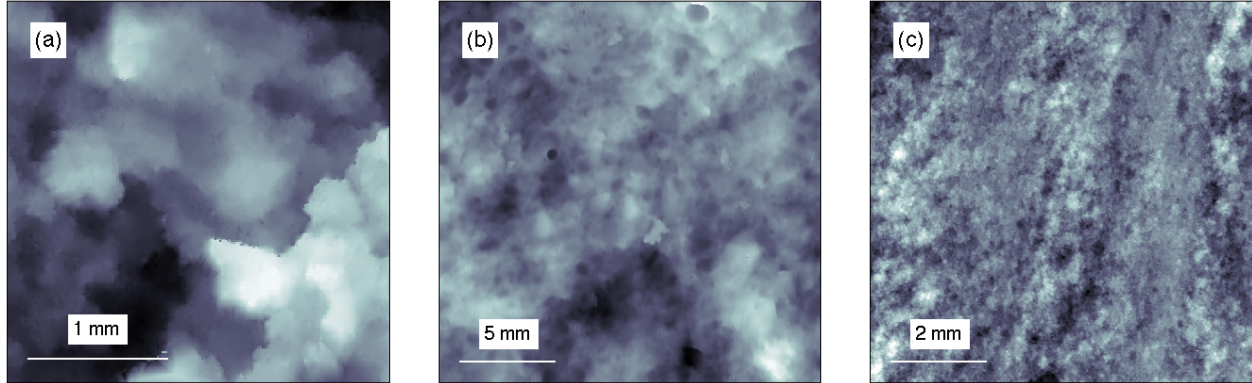


Figure 1: Fracture surfaces of (a) aluminum #2 (2.7×2.7 mm), (b) mortar (20×20 mm) and (c) a brittle ceramics (8×8 mm): the height of the surface is encoded using grey shades, with white representing the highest points while black corresponding to the lowest ones. The typical height denivelation on this surface is (a) 1.3 mm, (b) 2.3 mm and (c) $250 \mu\text{m}$, respectively.

the brittle ceramic sample (Fig. 2(c)), the distribution of height fluctuations shows an essentially Gaussian behavior at all scales. As the scale δr is increased, the standard deviation of the distribution is increased but the shape of the distribution remains essentially the same. The evolution of these distributions can be described by a family of Student t distributions (Fig. 2). The detailed analysis of this behavior will be presented elsewhere [4].

4 Spatial organization of large fluctuations on fracture surfaces

The distributions of height fluctuations in the materials investigated do not follow a Gaussian behavior because of the fat tails. In this part, we proceed to a detailed analysis of these extreme events or largest height variations that are present in an abnormally high proportion on fracture surfaces and that are directly responsible for these tails. Our analysis will reveal a fundamental difference between the morphology of fracture surfaces obtained by brittle failure, and the one obtained by damage mechanisms. It will also provide interesting clues on the origin of this deviation from the Gaussian behavior.

4.1 Revealing the spatial organization of the extreme events on fracture surfaces

The maps of extreme events with clusters are extracted from the fracture surface using the following procedure. We define the operator

$$\overline{\delta h}(\delta r, \vec{x}) = \langle [h(\vec{x} + \delta \vec{x}) - h(\vec{x})]^2 \rangle_{|\delta \vec{x}| = \delta r}^{\frac{1}{2}} \quad (1)$$

where the average $\langle \cdot \rangle$ is done on a circle of radius δr , i.e. for all admissible $\delta \vec{x}$ such as $|\delta \vec{x}| = \delta r$. This operator has several interesting properties. First, at a given scale δr , the operator is uniquely

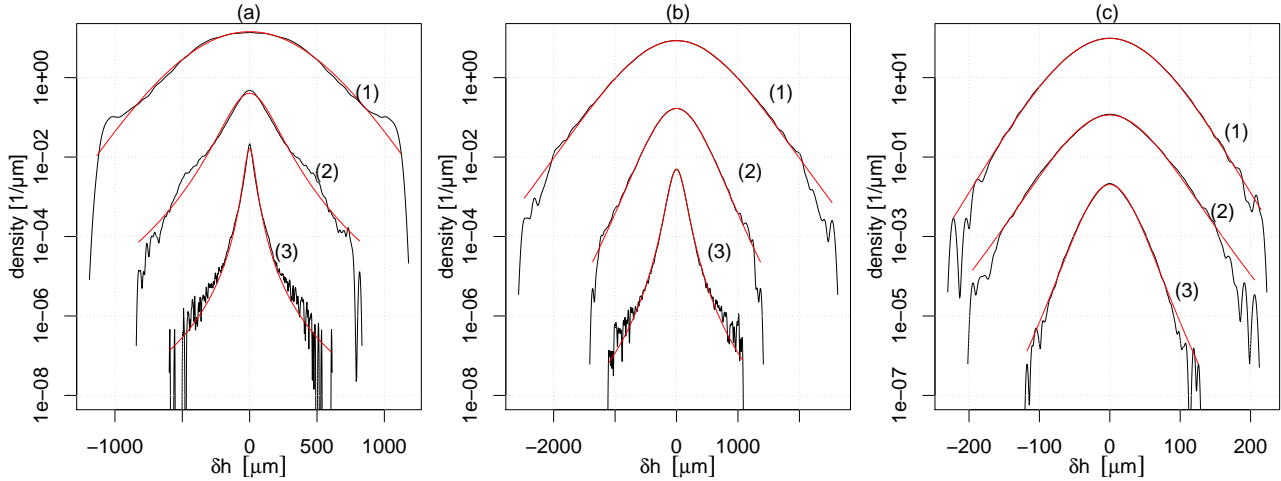


Figure 2: Distribution of height fluctuations $p(\delta h|\delta r)$ at various scales δr . (a) Aluminum alloy #2 with $\delta r = (1) 25 \mu\text{m}$, (2) $115 \mu\text{m}$, (3) $550 \mu\text{m}$; (b) Mortar sample with $\delta r = (1) 225 \mu\text{m}$, (2) $915 \mu\text{m}$, (3) 3.8mm ; (c) Brittle ceramic sample with $\delta r = (1) 60 \mu\text{m}$, (2) $310 \mu\text{m}$, (3) 1.5mm . The experimental distributions are represented in black, and the corresponding fit with a Student t distribution are represented in red/grey. For readability the distributions have been multiplied by 10^4 for (1) and by 10^2 for (2)

defined for each point of the experimental map and defines a transformation of the original map. Second, it is perfectly isotropic. Third, the average procedure makes it robust to measurement artifact. Qualitatively, this operator describes the local intensity of the height variation at a scale δr . The fields $\overline{\delta h}(\delta r, \vec{x})$ obtained from (a) the aluminum #2, (b) the mortar and (c) the ceramics fracture surfaces are represented on Fig. 3 at scale $\delta r = 6 \mu\text{m}$, $\delta r = 100 \mu\text{m}$ and $\delta r = 15 \mu\text{m}$, respectively. Here, the largest height variations are presented in white while the smallest ones are in black. Strikingly, the extreme events are spatially correlated and form a network of rough lines for the alloy [Fig. 3(b)] and the mortar [Fig. 3(c)], while they are rather uniformly distributed for the ceramic fracture surface [Fig. 3(a)]. At first sight, the differences between these maps are obvious. But to proceed to a quantitative analysis and describe their differences, we need to threshold these maps. As we are interested by the fat tails only, we define maps that contain the largest height variations only. As a result, we introduce a threshold δh_{th} so that for value of $\overline{\delta h}(\delta r, \vec{x})$ higher than h_c , we assign a value unity to the point \vec{x} (in white on Fig. 4), while a value zero is attributed to the points \vec{x} for which $\overline{\delta h}(\delta r, \vec{x}) < \delta h_{\text{th}}$ (in black on Fig. 4). Two parameters need to be chosen in order to obtain the maps of extreme events represented on Fig. 4: the value of δr that sets the scale at which the height variations $\overline{\delta h}(\delta r, \vec{x})$ are computed and the value of the threshold that distinguish the extreme events from the regular ones. In the following, instead of δh_c , we will use the quantity p_{th} that indicates the proportion of points \vec{x} with value $\overline{\delta h}(\delta r, \vec{x}) > \delta h_c$ defined as extreme events. Since we investigate the tail of the roughness distribution, typical values of p_{th} will be in the range 5% – 25%. In the following, we will see that the actual value of p_{th} as well as the value of δr have actually a limited influence on the statistical properties of the extreme events.

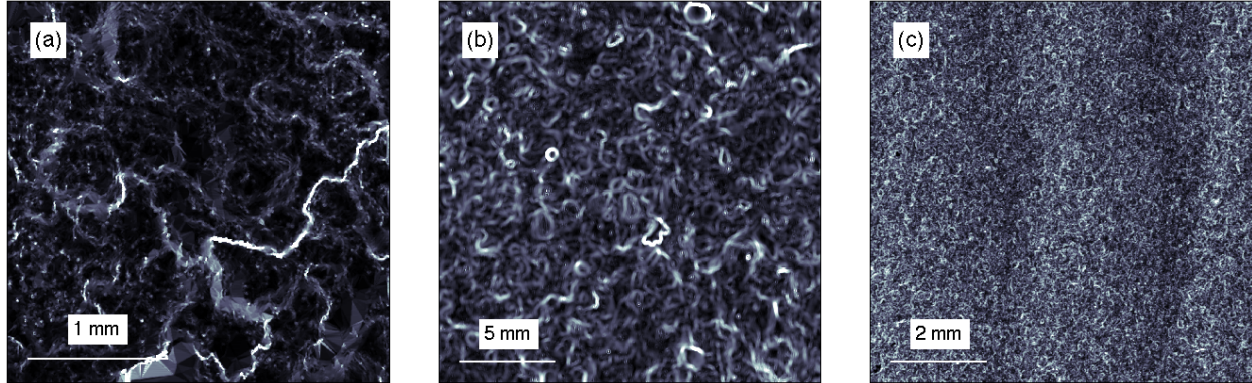


Figure 3: Maps of height variations $\overline{\delta h}$ computed on the fracture surfaces of (a) the aluminum alloy #2 for $\delta r = 6\mu\text{m}$, (b) the mortar and (c) the brittle ceramics shown on Fig. 1.

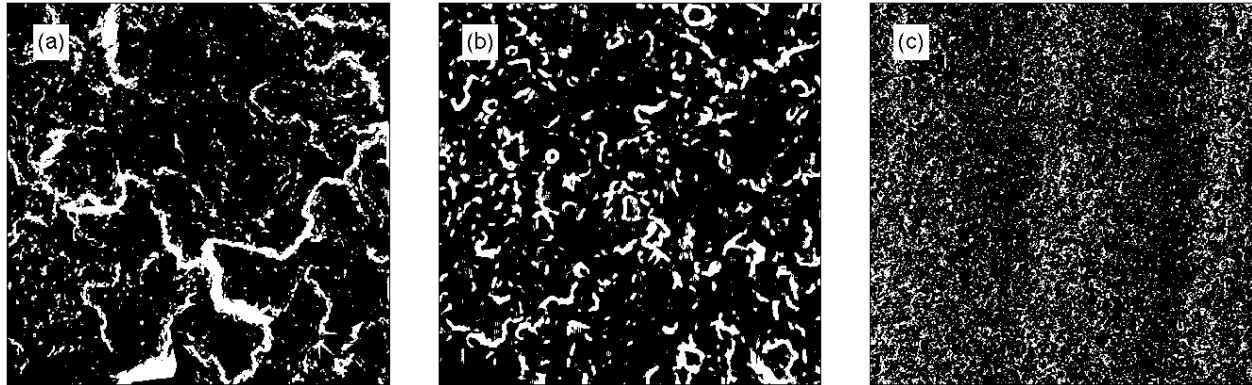


Figure 4: Threshold maps of the height variations $\overline{\delta h}$ shown on Fig. 3 computed on the fracture surfaces of (a) the aluminum alloy #2, (b) mortar and (c) brittle ceramics. Here, only the largest events that represents $p_{th} = 15\%$ of all the points on surfaces have been kept.

4.2 Statistical properties of clusters of extreme events

A rapid look at the spatial distribution of the extreme events shown on Fig. 4 shows that they organize in clusters of connected points. In this part, we investigate the properties of these clusters, such as their fractal dimension and their size distribution. For analyzing the cluster statistics, we define for each cluster isolated from the other ones three quantities that characterize their size, namely ℓ_x , ℓ_z and R_g , as well as one quantity S characterizing their area. ℓ_x is the maximum extent of the cluster along the x direction while ℓ_z is the maximum extent of the cluster along the z direction - let us note that x and z corresponds to the direction of the propagation, and the perpendicular one, respectively. R_g is the radius of gyration of the cluster. It is obtained by defining the center of gravity C of each cluster, and then compute the average distance between C and the points $\{M_k\}_{1 \leq k \leq N}$ belonging to the cluster, i.e. $R_g = \sqrt{\sum_{k=1}^N |C\vec{M}_k|^2}$ with $\sum_{k=1}^N C\vec{M}_k = 0$. For each cluster, we have so three variables characterizing its length while S defined as the total number N of of points of pixels that belongs to

the cluster times the area of one pixel represents its area. As shown on the Figs. 5 that shows the relation between length and area for each cluster for the , the three quantities ℓ_x, ℓ_z and R_g are found to follow the same scaling $S \sim \ell^D$ with the cluser area S . This indicates a fractal geometry of these objects with dimension $D \simeq 1.70$ that depends very weakly of the considered material (see Table 1 for the values of D of each material). This result indicates that any of the three quantities ℓ_x, ℓ_z and R_g can be used to investigate the cluster size distribution. In the following, we choose the radius of gyration. The probability distribution of the cluster sizes is shown on Fig. 6 for (a) aluminum alloy #1

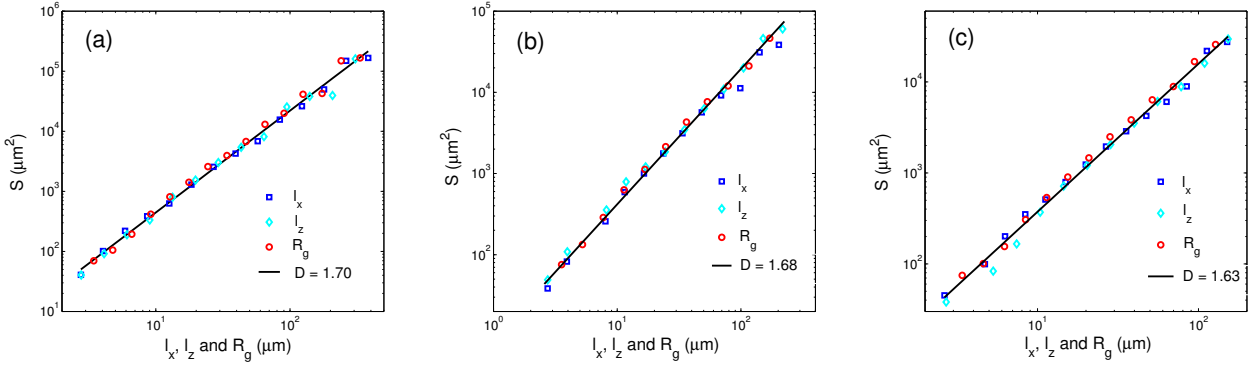


Figure 5: Relationship between length and area of the clusters of extreme events for (a) the aluminum #1, (b) the mortar and (c) the brittle ceramics. The scaling of the cluster rarea with its radius of gyration indicates a fractal dimension $D \simeq 1.70$, irrespective of the material considered.

and (b) mortar for different values of p_{th} for $\delta r = 6 \mu\text{m}$ and $\delta r = 100 \mu\text{m}$, respectively. Irrespective of the actual value of the threshold probability p_{th} , the distribution for mortar and aluminum fracture surfaces follow a power law $P(R_g) \sim R_g^{-\alpha}$ with exponent $\alpha \simeq 2.2$. The picture is rather different

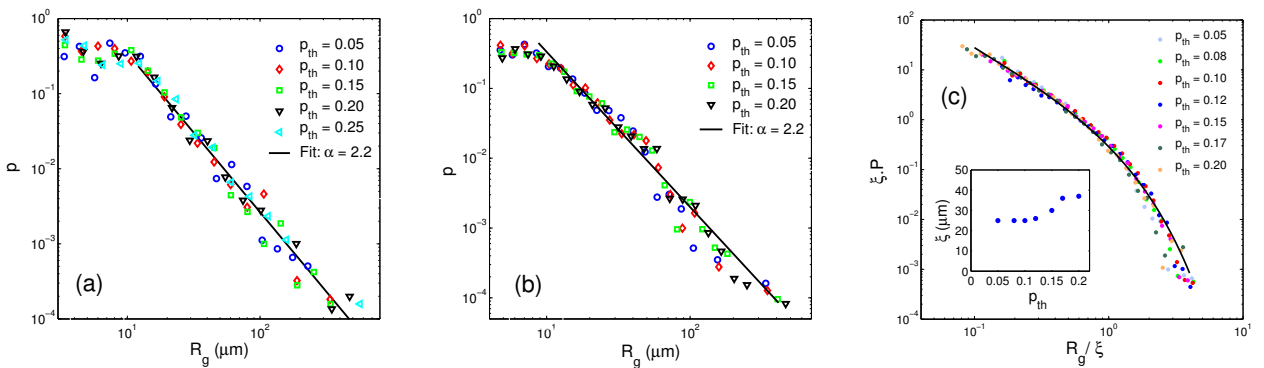


Figure 6: Distribution of cluster sizes R_g for (a) the aluminum alloy #1, (b) the mortar and (c) the brittle ceramics fracture surfaces.

for brittle fracture surfaces: as shown on Fig. 6(c) for $\delta r = 16 \mu\text{m}$, the distribution of cluster sizes follows an exponential law $P(R_g) \sim e^{-R_b/\xi}$ characterized by the length scale $\xi \simeq 25 \mu\text{m}$, the value of which depends very weakly of the threshold p_{th} , as shown in the inset of Fig. 6(c). This exponential

behavior confirms the visual observations made on Fig. 4: for ceramics fracture surfaces, the largest height variations do not form any large scale structures, contrary to mortar and aluminum. As a result, clusters of size larger than $\xi = 25 \mu\text{m}$ are exponentially rare. These results are confirmed on another brittle material, a natural sandstone. For its fracture surface also, the density probability of cluster size decreases exponentially, with a characteristic length scale $\xi \simeq 50 \mu\text{m}$ (see Table 1). This length might be directly related to the material microstructure since the grain size d in the ceramics and the sandstone are of the same order than this cut-off length, i.e. $d = 100 \mu\text{m}$ and $d = 200 \mu\text{m}$, respectively [5, 6]. We investigate now the effect of the length scale δr chosen to compute the field of height variations $\bar{h}(\delta r, \vec{x})$ on these properties. Figure 7 shows such maps obtained on the aluminum #1 fracture surface calculated at different scales, i.e. for (a) $\delta r = 6 \mu\text{m}$, (b) $\delta r = 12 \mu\text{m}$ and (c) $\delta r = 18 \mu\text{m}$. We see that changing this scale mainly affects the thickness of the lines constituting the network of extreme events, but does not really affect their geometry. This impression is confirmed on Fig. 8 where the statistical properties of the clusters obtained from these different maps are compared. The scale δr has a weak effect on both (a) the relation between the area and the radius of gyration of each cluster and (b) their size distribution. In other words, changing the scale δr in the range investigated does not affect significantly the value of the exponents $D \simeq 1.70$ and $\alpha \simeq 2.2$.

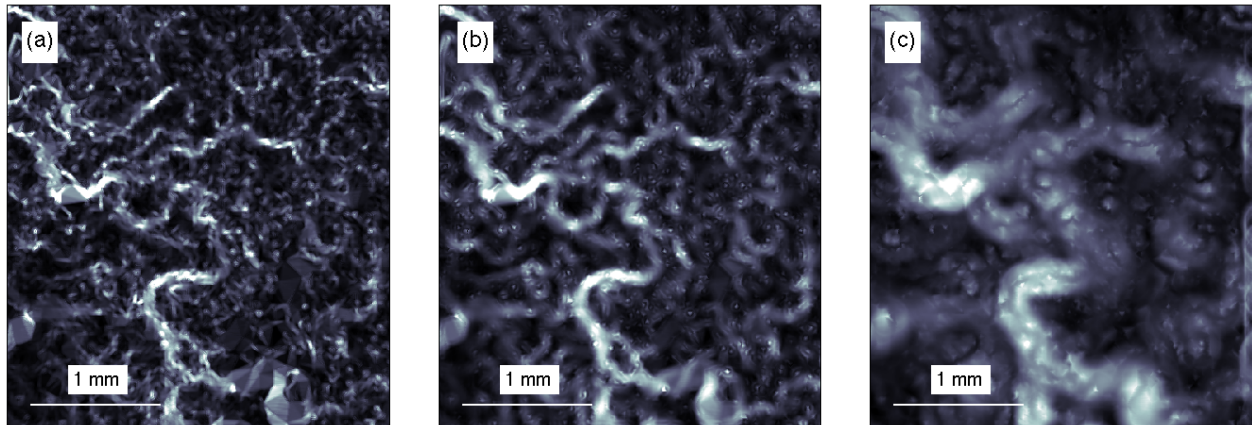


Figure 7: Map $\bar{\delta h}(\delta r, \vec{x})$ of height variations computed at different length scales (a) $\delta r = 6 \mu\text{m}$, (b) $\delta r = 12 \mu\text{m}$ and (c) $\delta r = 18 \mu\text{m}$ for the aluminum #1.

5 Discussion

We would like now to connect the statistical properties of the roughness showing deviations to the Gaussian behavior with the complex spatial distribution of extreme events observed on the height variations maps $\bar{\delta h}(\delta r, \vec{x})$. To bridge these both properties, it is relevant to consider the decomposition $\delta h(\vec{x}, \delta \vec{x}) = h(\vec{x}, \delta \vec{x}) - h(\vec{x}) = \sum_{k=1}^n h(\vec{x} + \frac{k}{n} \delta \vec{x}) - h(\vec{x} + \frac{k-1}{n} \delta \vec{x}) = \sum_{k=1}^n \delta h(\vec{x} + \frac{k-1}{n} \delta \vec{x}, \delta \vec{x}/n)$ that expresses a height variation calculated at the scale $\delta r = |\delta \vec{x}|$ in position \vec{x} as the sum of n height variations calculated at a smaller scale $\delta r/n$ near \vec{x} . For an uncorrelated map of height variations, the central limit theorem predicts then that the statistics of height variations - that writes as the sum

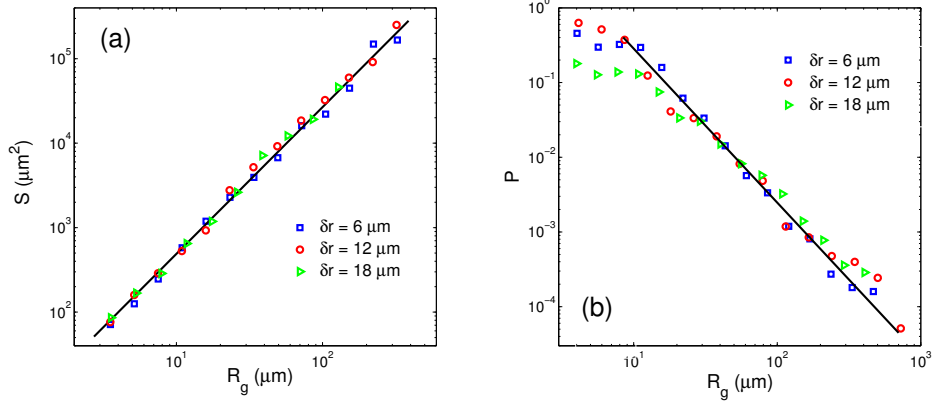


Figure 8: Effect of the length scale δr on the statistics of clusters of extreme events: (a) Relationship between area and length of clusters showing $D \simeq 1.70$ for the fracture surface of aluminum #1. (b) Distribution of cluster sizes R_g showing $\alpha \simeq 2.1$ on aluminum #1 fracture surface.

of uncorrelated variables - belongs to one of the three stable distributions, i.e. Gumble, Weibull or Gaussian distributions. Here, we expect the statistics of our fracture surfaces to follow a Gaussian distribution. This agrees with our observations made on brittle fracture surfaces that exhibit both Gaussian statistics and uncorrelated maps of height variations. On the contrary, quasi-brittle and ductile failure mechanisms that produce correlated height variations maps [Fig. 4 (a) and (b)] also display strong deviations to the Gaussian behavior. But once investigated at scales much larger than the typical size of those patterns, the height variations becomes uncorrelated, and so a Gaussian statistics might be expected: this explains the transition from fat tail distribution at small scale to a Gaussian statistics at large scales, as shown on Fig. 2. An analysis of the distribution $p(\delta h|\delta r)$ of height variations at different scales δr allows for an estimation of the crossover length $\delta r = \xi$ corresponding to the transition from fat tails to Gaussian statistics. Its value measured on mortar and the various aluminum alloys fracture surfaces is given in Table 1 . In this case, a typical value of the cluster size could not be extracted from their distribution as for brittle failure, due to the limited dimension of the fracture surfaces investigated. However, the previous connection between the roughness statistics and the patterns of extreme events suggests that the roughness recovers a Gaussian behavior once δr is much larger than the typical cluster size. This means that the length scale extracted from the cluster size distribution might be quite close to the crossover length between power law tail and Gaussian statistics. For this reason, we have used the same notation ξ whenever this length was extracted from the roughness statistics or the cluster size distribution. Our results show that that when fracture surfaces investigated at scales $\delta r \ll \xi$ display spatially correlated roughness characterized by a power law tail statistics, while investigated at scale $\delta r \gg \xi$, they follow a Gaussian behavior without exhibiting any spatial correlation on the height variations map. Interestingly, the deviations to the Gaussian behavior that are characterized by a change in the shape of the roughness distribution $p(\delta h|\delta r)$ with the scale δr results in a multi-affine behavior, that means that the various moments of this distribution scale with different exponents, contrary to mono-affine brittle surfaces for which one roughness exponent ζ is sufficient to fully describe the roughness statistics and the scaling of the different moments. Multi-scaling is classically associated with the presence of spatially correlated fluctuations. This in-

	ζ	D	α	ξ
Aluminum #1	0.74	1.70	2.2	450 μm
Aluminum #2	0.73	1.70	2.3	550 μm
Mortar	0.73	1.61	2.2	1.3 mm
Sandstone	0.45	×	×	25 μm
Ceramics	0.43	×	×	25 μm

Table 1: Scaling exponents extracted from the fracture surfaces resulting from ductile and quasi-brittle (upper part of the table) and brittle failure (lower part): the roughness exponent ζ characterizes the scaling behavior of the roughness correlation, the exponents D and α describe the patterns made by the largest height variations on the fracture surfaces presented on Fig. 4. The length ξ provides the crossover length between fat tail and Gaussian statistics for damage accompanied failure (alloy and mortar) while it gives the characteristic length of the exponential decay of the cluster size distribution for brittle failure.

terpretation is then fairly consistent with our observations. Let us note that this might also be the case in various other materials where multi-scaling were reported at small scale, before a transition towards a Gaussian behavior [7, 8]. We would like now to propose a physical interpretation of the length ξ and the origin of the complex features observed on the height variations maps. Various findings presented here suggest that the deviations to Gaussian statistics and the associated patterns of extreme events find their origin in the microcracking processes accompanying failure of mortar and aluminum alloys. This is supported by the following observations:

- (i) For mortar and aluminum fracture surfaces, abnormally large height fluctuations producing fat tail statistics of crack roughness organizes into a network of rough lines. This features are not present on brittle fracture surfaces for which damage mechanisms does not come into play, suggesting a direct link between clusters of extreme events and damage processes.
- (ii) The size of the clusters observed on the height variation maps is power law distributed, up to a cut-off length scale ξ that coincides well with the typical size associated with the damage processes in these materials: a few grain or a few hundreds of micrometers in aluminum alloy and a few millimeters in mortar. In addition, direct observations of the failure processes within the damage zone ahead of cracks in some quasi-brittle rocks show the presence of a forest of microcracks with power law distributed sizes. Direct observations have not been reported in mortar nor in aluminum alloys, but the acoustic emission following power law statistics in these materials suggest a similar behavior.
- (iii) In a recent study, networks of lines observed on PMMA fracture surfaces were shown to result from microcracking processes [9]. The mechanisms into play can be described by considering the coalescence of two interacting microcracks that start to avoid before attracting each to let a bump on the fracture surface [10]. Contrary to mortar or aluminum alloys, the PMMA is rather homogeneous at the scale where these lines where observed, allowing a straightforward observation, and even a quantitative interpretation of these features in terms of microcracking

history in the material [11]. In mortar and aluminum alloy, the network made by these lines is hidden by the surrounding roughness generated by the material heterogeneities. In addition, the microcrack density might be much larger in these materials, so that such an interpretation of the clusters observed for these materials is much more complex. However, they might be signature of microcracking and their size distribution might be closely connected with the size distribution of microcracks.

6 conclusion

The fracture surface investigated in this study revealed a much more complex roughness than their classical description based on the measurement of the roughness exponents. Neglecting for this study the anisotropy of fracture surfaces [12], we showed that one roughness exponent $\zeta \simeq 0.4$ remains sufficient to fully describe the roughness statistics. However, in quasi-brittle and ductile materials where the roughness exponent is found to be larger with $\zeta \simeq 0.75$, the full distribution of height variations is found to be highly non-Gaussian with the presence of fat tails. However, these deviations disappear as the investigation scale increases, leading to a Gaussian statistics at a sufficiently large scale. This behavior can be described with a family of Student's t distributions.

We proceeded then to the analysis of the largest height jumps on the surface, responsible for the fat tails observed in the roughness distribution. For this purpose, we defined maps of extreme events that displayed connected clusters of large fluctuations. These clusters of spatially correlated large fluctuations are shown to follow power law statistics: they have a fractal geometry with dimension $D \simeq 1.7$ with a power law distributed size with exponent $\alpha \simeq 2.2$. In brittle materials like sandstone and ceramics, the size distribution of these cluster follows a power law distribution characterized by the length scale ξ . In other words, we have a very small probability to find big clusters in brittle material that was shown to be in agreement with a Gaussian statistics.

The length scale ξ that we defined alternatively on quasi-brittle and ductile fracture surfaces from the crossover length from fat tail statistics at small scale to Gaussian statistics at large scale reveals the microscale failure mechanisms of materials. Our observations suggest that this length is connected with the typical length of micro cracks in materials. A possible interpretation is that the coalescence between micro cracks leads a signature on the fracture surface that we identified as abnormally large height fluctuations. According to this scenario, the length ξ extracted from the fracture surfaces might be connected to the typical damage zone size ahead of the crack during failure.

References

- [1] S. Vernède. A granular model of solidification as applied to hot tearing. *Ph.D. thesis*, 3795, EPFL, 2007.
- [2] S. Morel and D. Bonamy and L. Ponsons and E. Bouchaud. Transient damage spreading and anomalous scaling in mortar crack surfaces. *Phys. Rev. E*, 78:016112; 2008.
- [3] L. Ponsón and H. Auradou and P. Vié and J.-P. Hulin. Low self-affine exponents of fracture glass ceramics surfaces. *Physical Review Letters*, 87:105502, 2001.

- [4] S. Vernède, Y. Cao, L. Ponson. Non-Gaussian statistics and spatially-organized extreme events on experimental fracture surfaces. In preparation
- [5] L. Ponson, H. Auradou, M. Pessel, V. Lazarus and J.-P. Hulin. Failure mechanisms and surface roughness statistics of fractured Fontainebleau sandstone. *Phys. Rev. E*, 76:036108, 2007.
- [6] L. Ponson, H. Auradou, P. Vié and J. P. Hulin. Low self-affine exponents of fractured glass ceramics surfaces. *Phys. Rev. Lett.*, 97:125501, 2006.
- [7] S. Santucci, K. J. Måløy, A. Delaplace, J. Mathiesen, A. Hansen, J. Bakke, J. Schmittbuhl, L. Vanel and P. Ray. Statistics of fracture surfaces. *Phys. Rev. E*, 75:016104, 2007.
- [8] E. Bouchbinder, I. Procaccia, S. Santucci and L. Vanel. Fracture surfaces as multiscaling graphs. *Phys. Rev. Lett.*, 96:055509, 2006.
- [9] J. Scheibert, C. Guerra, F. Célarié, D. Dalmas and D. Bonamy, Brittle-qausibrittle transition in dynamic fracture: An energetic signature. *Phys. Rev. Lett.*, 104:045501, 2010.
- [10] M. L. Fender, F. Lechelault and K. E. Daniels. Universal shapes formed by two interacting cracks. *Phys. Rev. Lett.*, 105:125505, 2010.
- [11] C. Guerra, J. Scheibert, D. Bonamy and D. Dalmas. Understanding fast macroscale fracture from microcrack post mortem patterns. *Proc. Nat. Acad. Sci.*, 109:390-394, 2012.
- [12] L. Ponson, D. Bonamy and E. Bouchaud. Two-dimensional scaling properties of experimental fracture surfaces. *Phys. Rev. Lett.*, 97:125501, 2006.